THE JOURNAL OF PHYSICAL CHEMISTRY C

Article

Cite This: J. Phys. Chem. C 2018, 122, 26974−26986

pubs.acs.org/JPCC

Multiscale Approach to the Dissociative Adsorption of Oxygen on a Highly Dispersed Platinum Supported on γ-Al_2O_3

Alexis Sangnier,[†] Mickaël Matrat,[†] André Nicolle,[†] Christophe Dujardin,[‡] and Céline Chizallet*[,§]

[†]Powertrain and Vehicle Division, IFP Energies nouvelles, Institut Carnot IFPEN Transports Energies, 1 et 4 avenue de Bois-Préau, 92852 Rueil-Malmaison Cedex, France

[‡]Univ. Lille, ENSCL, Centrale Lille, CNRS, Univ. Artois, UCCS UMR 8181, 59000 Lille, France

[§]IFP Energies nouvelles, Rond-point de l'Echangeur de Solaize, BP 3, 69360 Solaize, France

Supporting Information

ABSTRACT: The understanding of the reactivity of supported platinum with oxygen is of paramount relevance in heterogeneous catalysis, inter alia. We present here a multiscale investigation of the interaction of highly dispersed Pt/γ-Al_2O_3 catalysts with O_2, through the combination of temperature-programmed desorption (TPD) experiments, ab initio simulations on a model Pt_{13}/γ-Al_2O_3 cluster, and kinetic simulations of the TPD, thanks to data obtained from ab initio calculations. The specific behavior of the sub-nanometric platinum particles is benchmarked against the one of the ideal Pt(111) surface, as predicted by similar ab initio-based kinetic modeling. This approach reveals a fully different reactivity of highly dispersed Pt nanoparticles with respect to Pt(111), with a much higher capacity of oxygen storage for given temperature and $P(O_2)$ conditions. In a large operating conditions interval, the Pt_{13} clusters are converted into an oxide, whose stoichiometry is close to PtO_2, but with a very specific hemispherical shape. $Pt_{cluster}$−$O_{alumina}$ and $O_{cluster}$−$Al_{alumina}$ bonds ensure a very strong interaction of these clusters with the support. The kinetic scheme built upon ab initio data to simulate TPD experiments allows to attribute the highest desorption temperatures reached experimentally to highly dispersed particles, from $Pt_{13}O_{20}$ to $Pt_{13}O_4$ clusters, through $Pt_{13}O_{16}$ and $Pt_{13}O_{10}$ intermediates.

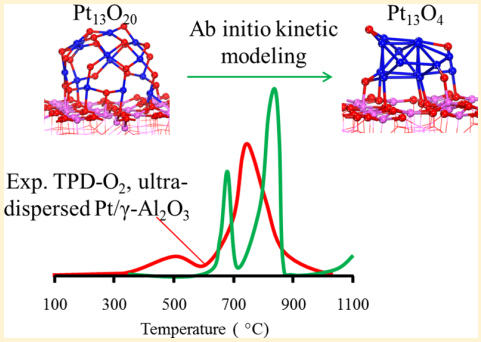

1. INTRODUCTION

Platinum is a widely used active phase in heterogeneous catalysis due to its intrinsic activity for hydrogenation/dehydrogenation reactions, as well as its redox properties.[1−4] It is involved in many environmental, refining, and petrochemical applications.[5−8] Regarding automotive applications, post-treatment devices contain different metals such as rhodium, palladium, and platinum, enabling the oxidation of hydrocarbons and carbon monoxide in CO_2.[9] Platinum also contributes to the conversion of chemical energy into electricity, assisting the hydrogen oxidation to water in fuel cells.[10−13] Platinum is also involved into CO conversion to CO_2 and H_2 through the well-known water−gas shift reaction.[9] Recently, EU listed platinum as a critical material because the supply of the platinum group metals (PGMs) is still relatively concentrated within few countries.[14] The optimization of high dispersions is a way to reduce practically the use of PGMs.

Understanding the catalyst structuration effect on its reactivity and selectivity is then decisive. In particular, size effects play a huge role in many properties of nanoparticles, with respect to bulk materials.[15−18] These effects are also expected to vary significantly according to the environment of the catalyst, such as the nature of the support or the nature of the gas. For example, the Pt(111) surface is considerably changing in the presence of O_2, from dissociative adsorption on hollow face-centered cubic (fcc) sites[19−23] to PtO_2 layers,[24−26] or, depending on temperature and O_2 partial pressure, to more special surface structures such as triangles,[27] honeycombs,[28] or spoke wheels.[29] A structure effect of platinum for the interaction of O_2 is already known: in the case of Pt(321) and Pt(211), the presence of steps or adatoms influences the adsorption of oxygen.[30,31] These atoms facilitate the adsorption at low coverage and lead to higher heats of adsorption than Pt(111). The particle size was also shown to have a drastic impact on oxygen retention for supported platinum catalysts, which plays a major role in structure-sensitive oxidation reactions.[32−34]

In the present work, we focus on the interaction of O_2 with the Pt/γ-Al_2O_3 system, starting from well-dispersed catalysts with sub-nanometric metallic particle sizes. This is of interest for all the applications where platinum is used in oxidizing environment, such as for oxidation reactions, but also considering that most reduced platinum catalysts are obtained first in an oxidic form after impregnation, drying, and possible calcination.[35] Moreover, adsorption of oxygen on platinum particles is also a way to investigate the dispersion of a

Received: September 20, 2018
Revised: October 29, 2018
Published: November 1, 2018

DOI: 10.1021/acs.jpcc.8b09204
J. Phys. Chem. C 2018, 122, 26974−26986

catalyst.[36−39] γ alumina is a versatile nonreducible support, often chosen at the industrial and laboratory scale for its high surface area and significant surface reactivity,[40] allowing for the dispersion of small metallic particles, if not single atom catalysts.[41−44] Our aim is to get an atomic-scale insight into the surface structures described by the ultradispersed Pt/γ-Al_2O_3 system in the presence of O_2 and into the strength of the corresponding interaction.

Ab initio modeling appears as a relevant tool for the investigation of well-dispersed platinum particles on various oxides, in particular γ-Al_2O_3.[12,45,46] Thanks to density functional theory (DFT) calculations, small nonsupported aggregates from Pt_2 to Pt_{20}[47−50] were shown to reconstruct easily upon O_2 adsorption, which makes the adsorption strongly favorable. The preferred adsorption mode on these structures is the bridge one. For particles larger than Pt_{35},[51] regular facets such as Pt(111) or Pt(100) surfaces can be identified, contrary to the very distorted morphology of the smallest clusters.[52,53] The heat of adsorption of oxygen on the facets is of the same order of magnitude as that on the extended surfaces alone. The adsorption of atomic oxygen however appears to be preferred at the intersections of these facets such as edges and corners, thanks to the low-coordinated platinum at the edges combined with platinum atoms mobility. Systematic DFT calculations for clusters of variable size show that size effect is substantial for the adsorption of oxygen below about 150 atoms.[54] Although many DFT studies deal with the adsorption of oxygen on flat or corrugated platinum surfaces,[20,21,26,30,55−60] studies taking into account the support effect on the interaction of oxygen with platinum clusters are much scarcer, and generally concern very small clusters or single atoms and a single O_2 molecule.[47,61,62] A systematic investigation of the interaction of oxygen with sub-nanometric platinum cluster, typically Pt_{13}, supported on γ-Al_2O_3, taking into account the effect of O coverage, function of the temperature and O_2 partial pressure, and possible reconstructions, is thus needed. The approach previously undertaken in the case of hydrogen interaction with Pt_{13}/γ-Al_2O_3, revealing strong reconstructions of the metallic phase and modulation of the metal−support interaction upon variation of the H coverage,[41,63] is worth being extended to oxygen.

In the present work, we propose to combine ab initio periodic calculations and O_2 temperature-programmed desorption (TPD) measurements, the respective consistency of which will be evaluated thanks to kinetic modeling, based on the ab initio data, through a multiscale simulation approach. Although such an approach turned out to be successful in the case of oxygen desorption from Pt(111)[58] and for many other chemical systems,[64−75] it was never demonstrated for the interaction of oxygen with the ultradispersed Pt/γ-Al_2O_3 system so far. First, a systematic structural investigation is provided for O_2 dissociative adsorption on Pt_{13}/γ-Al_2O_3(100) for a number of oxygen atoms per cluster ranging from 1 to 32, thanks to ab initio molecular dynamics (MD). Our own calculations on the Pt(111) surface allow the comparison with highly dispersed platinum using the same approach. Thermodynamic and kinetic data are extracted from these ab initio models, which allow us to build a kinetic model to simulate the TPD experiments. This multiscale approach leads to a full assignment of the experimental feature in terms of particle size and oxygen coverage.

2. METHODS AND EXPERIMENTAL DETAILS

2.1. Ab Initio Calculations. Structure optimizations were performed with the Vienna ab initio simulation package (VASP).[76,77] A plane-wave basis set using the projector-augmented wave[78] was employed. The generalized gradient approximation Perdew−Burke−Ernzerhof exchange correlation functional[79] was used for the whole study. The cutoff energy for the plane-wave basis was set to 400 eV. Gaussian smearing with σ = 0.02 eV was used for the supported clusters. The electronic optimizations were done up to a convergence of 10^{-6} eV for the self-consistent loop and geometries were optimized until all forces on atoms were lower than 0.02 eV/Å. Dipolar correction was added in the direction perpendicular to the slab. Bader charges[80,81] were calculated at the same level of theory.

For the cluster system, we chose the dehydrated γ-Al_2O_3(100) surface model of Digne et al. as the support model.[82,83] Indeed, from previous studies about monometallic or bimetallic catalysts, models involving γ-Al_2O_3(100) dehydrated surface as a first approach already provided fruitful detailed information.[41,45,53,63,84] A two-platinum-layer Pt_{13} structure was found to be the most stable on this alumina facet.[53] The box dimensions (16.71 × 16.79 × 21.80 Å^3) were chosen to avoid lateral interactions between periodic cluster images. Periodic slabs consist of four alumina layers separated by a vacuum thickness corresponding to more than two equivalent empty layers. The two topmost alumina layers were relaxed, as well as all metallic atoms, whereas the two other alumina ones were frozen. Calculations were performed at the Γ point. For the Pt(111) model, a 3 × 3 five-layer slab model was used, with a 5 × 5 × 1 *K*-points grid. The top three layers were relaxed, whereas the two others were frozen.

The adsorption energies of atomic oxygen were calculated per O_2 molecule, according to eq 1. The energy of O_2 (E_{O_2}) was calculated by placing a O_2 molecule into a 15 × 15 × 15 Å^3 box.

$$E_{\text{adsorption}} = \frac{2}{n}\left(E_{\text{Pt}\{i\}\text{O}_n} - E_{\text{Pt}\{i\}} - \frac{n}{2}E_{\text{O}_2}\right) \quad (1)$$

n is the number of oxygen adsorbed per cell on Pt_{13} or Pt(111) and $E_{\text{Pt}\{i\}\text{O}_n}$ and $E_{\text{Pt}\{i\}}$ are the electronic energies of the system considered with or without adsorbed oxygen, respectively (supported Pt_{13} cluster or Pt(111) surface). Energies presented in this work are displayed in kcal mol^{-1} per O_2 molecule and computed negatively when the reaction is favorable. In the case of n > 2, eq 1 gives the arithmetic mean adsorption energy per O_2.

In the case of the supported Pt_{13} cluster, with a number of oxygens higher than 1, four geometries were first optimized to determine the most stable one. The latter was then refined by velocity-scaled molecular dynamics (MD) at 600 K, with a time-step of 5 fs over 1500 steps, the whole alumina support being frozen for such calculations. In the course of the dynamics, very significant geometry changes were observed for most stoichiometries, sometimes with reconstruction of the cluster (Supporting Information S1). The three most stable geometries obtained during the MD run were then chosen to be quenched by performing a structure optimization calculation with the same characteristics as previously detailed.

For the alumina-supported cluster model, the interaction energy between the support and the platinum cluster was calculated by eq 2.

DOI: 10.1021/acs.jpcc.8b09204
J. Phys. Chem. C 2018, 122, 26974−26986

$$E_{\text{interaction}} = (E_{Pt_{13}O_n/\gamma\text{-}Al_2O_3} - E^*_{Pt_{13}O_n} - E^*_{\gamma\text{-}Al_2O_3}) \quad (2)$$

with single point calculations (referred to as a star superscript) for the separate cluster and support systems at the geometry of the supported system.

The thermodynamic diagram was built from the most stable quenched geometries obtained after molecular dynamics. Vibrational parts of the enthalpy and entropy were determined by an harmonic frequency analysis. This was performed with a displacement of ±0.01 Å in each direction for all relaxed atoms in the cell (same as for geometry optimizations). The Hessian matrix was then calculated by the finite-difference method. The entropy of this condensed phase was assumed to result only from its vibrational part, neglecting the rotational and translational degrees of freedom. The calculation of the free energy for each system was done using the equations reported in the Supporting Information S2. The oxygen-adsorption free energy $G_{\text{adsorption}}$ (cumulated over all adsorbed oxygen molecules) used to build the thermodynamic diagrams is given in eq 3. The different domain of coverages present on the diagrams reflects the minimum free energy among other coverage systems.

$$G_{\text{adsorption}}(p_{O_2}, T, \theta_{O_2}) = \left(G_{Pt_{13}O_n}(T, \theta_{O_2}) - G_{Pt_{13}}(T) - \frac{n}{2}G_{O_2}(p_{O_2}, T)\right) \quad (3)$$

Concerning the transition states identification for the dissociation of adsorbed O_2, the nudge elastic band (NEB) method was used.[85] The convergence criterion for the relaxation loop was set to 0.02 eV/Å. The initial guess for eight intermediate images was determined by Opt'n Path[86] via a Cartesian translation of the atoms from the initial to the final state. After the completion of the NEB optimization, a quasi-Newtonian[87] calculation was performed on the image that was the closest to the transition state. A vibrational calculation was finally done to validate the transition structure, with a single imaginary vibrational mode corresponding to the reaction studied.

2.2. Kinetic Modeling. The Chemkin Pro software[88] was used to simulate TPD from ab initio thermokinetic data. A perfectly stirred reactor was used as the reactor Peclet number was much lower than unity. Thiele and mass Biot numbers were found to be also much lower than one, highlighting the occurrence of kinetic regime. Hence, the diffusion phenomena of gas species to the surface were not taken into account.

The reaction mechanisms was built by including successive dissociative adsorption reactions of one molecule of O_2 according to eqs 4 and 5. Each direct and reverse reactions are listed, up to 32 oxygen atoms for Pt_{13} and 1 ML (monolayer) for Pt(111).

$$Pt_{13}O_n + O_2 \rightleftarrows Pt_{13}O_{n+2} \quad (4)$$

$$2\,Pt^* + O_2 \rightleftarrows 2O^* \quad (5)$$

It should be noted that in the case of $Pt_{13}O_n$ systems, the elemental site considered in the microkinetic calculations corresponds to one Pt_{13} particle with a global energetics. This differs from the Pt(111) scheme for which each platinum was considered as one site.

The rate constants of dissociative−adsorption reactions were computed using a sticking coefficient s, as detailed in eq 6, Γ_{tot} (cm^{-2}) standing for the number of free sites, m the reaction order, and $E_{\text{dissociation}}$ the activation energy needed for the dissociative adsorption to occur.

$$k_{\text{adsorption}} = \frac{s}{\Gamma_{\text{tot}}^{\ m}}\sqrt{\frac{RT}{2\pi M_{O_2}}}\exp\left(-\frac{E_{\text{dissociation}}}{RT}\right) \quad (6)$$

Notably, such a mean-field model does not take into account the need to have two neighboring sites for O_2 dissociation into two atomic oxygen. Such a need was shown recently in ref 89. This approach also does not indeed take into account surface species transport phenomenon, such as migration. Taking all these aspects into account would require a kinetic Monte Carlo simulation, for example, which is beyond the scope of the present work. Likely, the rates evaluated in the present work might be overestimated due to the absence of condition to have two neighboring free sites in the model. Part of the gap between the model and reality may be compensated by the choice of sticking factor values, for which we do not have any accurate experimental determination.

To account for coverage-dependent dissociation energy, a linear law was applied to the dissociation energies found for Pt(111), whereas piecewise linear trends were applied to the three ab initio dissociation energies investigated on the Pt_{13} cluster (see later, Section 4.3).

Thermodynamic consistency was guaranteed by eq 7, with $\Delta_r H_{\text{desorption}}$ and $\Delta_r S_{\text{desorption}}$ being the average enthalpy and entropy of the desorption reaction, respectively, determined between 300 and 1000 K with ab initio simulations between two consecutive oxygen coverage structures.

$$k_{\text{desorption}} = k_{\text{adsorption}} \times \exp\left(-\frac{\Delta_r H_{\text{desorption}} - T\Delta_r S_{\text{desorption}}}{RT}\right) \quad (7)$$

Few studies investigated the sticking coefficient of O_2 on Pt(111);[22,90,91] however, it was shown to vary strongly with O_2 partial pressure and temperature. No temperature deviation from the setpoint was detected experimentally, implying that the endothermic effect due to desorption may be neglected.

The desorption rate constants were fitted to the Arrhenius−Kooij formalism represented by eq 8.

$$k = A \times T^{\beta} \times \exp\left(-\frac{E_{\text{activation}}}{RT}\right) \quad (8)$$

A, β, and $E_{\text{activation}}$ denote, respectively, the pre-exponential factor, the temperature exponent, and the activation energy (in kcal mol^{-1}).

2.3. Experiments. *2.3.1. Preparation of the Catalysts.* Ultradispersed platinum catalysts were obtained by impregnation of a H_2PtCl_6 solution (STREM Chemical, 99.9 wt % purity, concentration adjusted to reach 0.3 and 1 wt % Pt) on γ-Al_2O_3 (Brunauer−Emmett−Teller surface equal to 200 $\text{m}^2\ \text{g}^{-1}$, obtained from the calcination of a SB3 boehmite gel from SASOL, same protocol as in ref 92), followed by drying at 120 °C overnight, and calcination at 520 °C under dry air (1 L g^{-1} h^{-1}) for 2 h, dechlorination by a wet air flow (8000 ppm h^{-1} water) at 520 °C. The dechlorinated samples were finally reduced under H_2 flow (1 L g^{-1} h^{-1}, 2 h) at 500 °C.

2.3.2. Characterizations. The catalysts were characterized by X-ray fluorescence (Thermo scientific ARL Perform'X) to determine the final platinum and chlorine content. The results are presented in the Supporting Information S3 and show that

DOI: 10.1021/acs.jpcc.8b09204
J. Phys. Chem. C 2018, 122, 26974−26986

the expected compositions are reached (close to 0.3 and 1 wt % for platinum, low chlorine loadings).

Platinum dispersion was determined by hydrogen titration of chemisorbed oxygen (H_2−O_2 titration) in a Gira Xsorb apparatus with a thermal conductivity detector. The samples were first calcined under air at 530 °C for 2 h at 10 °C min^{-1}. The sample then was cooled down to room temperature and purged with He. The first reduction with H_2 was done at 450 °C for 2 h with a flow of 87 NmL min^{-1} and a ramp of 5 °C min^{-1}. After cooling down to room temperature and purging with He, pulses with pressures from 0.5 to 60 kPa of oxygen were added until saturation occurred at 35 °C. This process was repeated once.

High angle annular dark field-scanning transmission electron microscopy (STEM) experiments were performed on a STEM/TEM JEOL 2100F microscope operating at 200 kV with a spot size of 0.5 nm. The reduced catalyst sample was grinded, suspended in ethanol, and sonicated. A drop of the resulting suspension was deposited on a copper grid coated with a holey-carbon film and the alcohol was evaporated.

2.3.3. O_2 Temperature-Programmed Desorption. The TPD experiments were performed with a Micromeritics (Autochem II 2920) setup. The oxygen release was quantified with a mass spectrometer (Pfeiffer QMS 200). The experiments occurred in three steps, with a total gas flow set to 50 mL min^{-1}: (1) a pretreatment step at 600 °C during 5 h with helium enables to remove adsorbed water as well as to clean the surface from adsorbates present on the catalyst and on the metal oxide; (2) a contact step with O_2 (mixture of 5% v/v O_2/He) during 1 h at 100 °C; (3) finally, the release of molecular oxygen is followed during the increase of temperature with a ramp of 5 °C min^{-1} using helium as a carrier gas. The temperature and duration of the pretreatment step were optimized after the analysis of the behavior of the 1 wt % Pt/γ-Al_2O_3 material (Supporting Information S4). The mass spectrometry signals of O_2 for alumina alone was moreover substracted from that of the catalysts obtained with the same treatment conditions to extract the contribution of the metallic particles alone.

3. EXPERIMENTAL RESULTS

3.1. Dispersion of Platinum Nanoparticles. The platinum nanoparticles supported on Al_2O_3 were characterized after synthesis and reduction with scanning tunneling electronic microscopy. Figure 1 presents the picture recorded for the 0.3 and 1 wt % platinum fresh catalyst.

The average particle size is 0.85 ± 0.18 and 1.07 ± 0.17 nm, respectively, for 0.3 and 1 wt % Pt/γ-Al_2O_3 catalysts (Figure 2), underlining the formation of highly dispersed nanoparticles supported on alumina. The average particle size corresponds to about ten-atoms platinum particle. Moreover, the H_2/O_2 titration performed gives a 0.98 and 0.90 dispersion, respectively, for the 0.3 and 1 wt % Pt/ γ-Al_2O_3 catalysts.

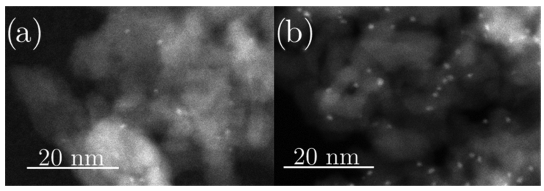

Figure 1. Scanning tunneling electronic microscopy of the fresh (a) 0.3 wt % Pt/γ-Al_2O_3 and (b) 1 wt % Pt/γ-Al_2O_3 catalysts after dechlorination.

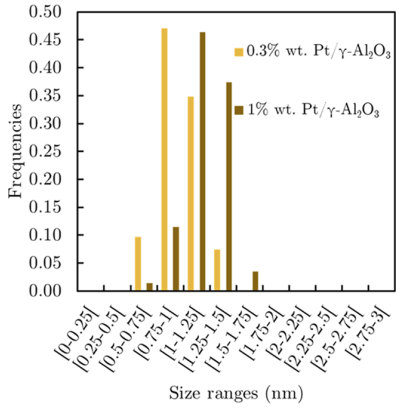

Figure 2. Particle size distribution of the fresh 0.3 and 1 wt % Pt/γ-Al_2O_3 catalysts after dechlorination (respectively 143 and 289 items probed).

3.2. O_2-TPD Experiments. For the 1 wt % Pt/Al_2O_3 catalyst, O_2 desorption is detected mainly at 504 and 757 °C (Figure 3). The peaks deconvolution with a Gaussian fit allows to put into evidence a shoulder at 835 °C (Supporting Information S5). The main peak is shifted to 710 °C on the 0.3 wt % Pt/Al_2O_3 catalyst, whereas shoulders are detected at 515 and 931 °C. In quantitative terms, the system with the lowest Pt content (0.3 wt % Pt) leads to an enhancement of the highest temperature peak and a decrease of the lower temperature peak as compared to the system with the highest Pt content (1 wt %).

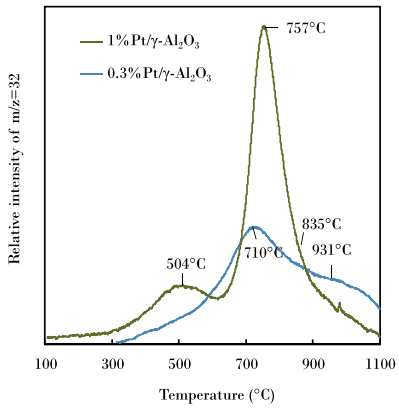

Figure 3. Relative intensity of oxygen (m/z = 32) during the temperature-programmed desorption with the 0.3 and 1 wt % Pt/γ-Al_2O_3 catalysts.

Parker et al. report the TPD of O_2 on Pt(111) with different initial oxygen coverages.[93] They show that for coverages lower than 0.2 ML, only one peak appears at around 460−540 °C. A second peak at 400 °C is noticed for higher oxygen coverages and a third lies at 120 °C for the initial oxygen coverages above 0.5 ML. No desorption is reported above 680 °C. For stepped surfaces,[94] a similar pattern is observed with peaks lying between 300 and 600 °C, with two peaks close to 400 and 500 °C. Our results show that the desorption of oxygen on highly dispersed platinum particles supported on alumina occurs on a

DOI: 10.1021/acs.jpcc.8b09204
J. Phys. Chem. C 2018, 122, 26974−26986

completely different range of temperature. This suggests that the platinum dispersion has a huge impact on oxygen interaction with platinum, thus on O_2 desorption profile. The shift in O_2 desorption peaks toward high temperature can be associated with stronger interactions between oxygen and platinum atoms in the case of highly dispersed platinum particles on alumina. In previous reports dealing with more or less dispersed Pt/Al_2O_3 catalysts, the main desorption peaks appeared below 500 °C, but temperatures higher than 700 °C were generally not sampled.[34,95,96]

4. AB INITIO SIMULATION OF OXYGEN ADSORPTION REACTIONS

Ab initio electronic structures calculations were undertaken on $Pt_{13}O_n/\gamma$-Al_2O_3 model to simulate the behavior of a highly dispersed platinum. Pt(111) was also considered to compare with the behavior of large particles or ideal metal surfaces. It also provides a good reference case (Supporting Information S6).

4.1. Adsorption of Atomic Oxygen. The 13-platinum atoms particle model is supported on a (100) γ alumina surface model.[53] The particle is composed of two layers of platinum atoms, among which 12 atoms out of 13 are a priori accessible to external molecules. This corresponds to a theoretical dispersion of 0.92. This small particle implies a nonregular surface on which no typical extended surface emerges.

Due to the absence of symmetry, each platinum atom and thus each site has a unique behavior. First, we simulated about 60 potential adsorption sites for oxygen (top, bridge, and hollow sites) by geometry optimization. Among the simulated configurations, some of them evolved into more stable ones. The adsorption energies obtained are summarized in Figure 4. Their average, by adsorption mode (as detailed below), is given in Table 1. Some of these structures are shown in Figure 5.

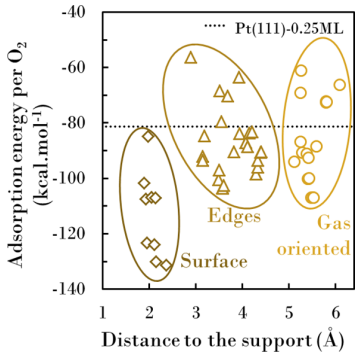

Figure 4. Adsorption energies per O_2 for a single O atom on the supported Pt_{13} cluster as a function of the distance to the support compared to Pt(111)-0.25 ML. The distance to the support corresponds to the difference of z-coordinates between the oxygen and the mean aluminum of the first alumina layer.

From Figure 4, three groups emerge according to their distance from the support. A first group, close to alumina (from 1 to 2.5 Å) is composed of the more stabilizing sites for atomic oxygen. This group corresponds to nonexpected adsorption sites that involve the alumina support. Figure 5d shows one of these structures, with the oxygen bonded to one platinum and one aluminum atom. Such a site is hereafter named bimetallic bridge. The bimetallic hollow site (Figure 5e) is composed of two platinum atoms and one aluminum. These peculiar sites that involve the support stabilize drastically the adsorbed oxygen atoms. Two bimetallic hollow sites and two bimetallic bridge sites stand out by their heat of adsorption over −120 kcal mol^{-1}, compared to the average −90 kcal mol^{-1} for typical sites.

The second group of sites, exhibiting a distance to the surface between 2.5 and 4.4 Å, involve two layers of platinum. They correspond to oxygen atoms adsorbed on the edges of the cluster. The adsorption energies are dispersed (from −60 to −100 kcal mol^{-1}), but they are significantly less negative in average as compared to the first group. The third group includes the farthest sites, i.e., located on the top of the particle (gap with the second group: 0.75 Å). The oxygen atoms are

Table 1. Average Adsorption Energy per O_2 at Low Oxygen Coverage

adsorption mode	adsorption mode	$E_{adsorption}$ (kcal mol^{-1})
$Pt_{13}O$—this work	top	−89.8
	bridge	−83.9
	hollow	−87.7
	bimetallic bridge (Al, Pt)	−108.1
	bimetallic hollow (Al, 2Pt)	−122.8
Pt(111)—this work	0.25 ML	−81.3
Pt(111)[20]	0.25 ML fcc hollow	−47.5
Pt(111)[21]	0.25 ML fcc hollow	−69.6
Pt(321)[30]	near-edge fcc hollow	−67.2
nonsupported Pt_xO_x[49]	top	−75.2 (x = 1)
	top, bridge	−79.4 (x = 2)
	bridge	−79.8 (x = 3)
	bridge	−88.4 (x = 4)
	bridge	−86.8 (x = 5)
	top, bridge	−112.6 (x = 10)
nonsupported Pt_{13}[48]	top	−60.9

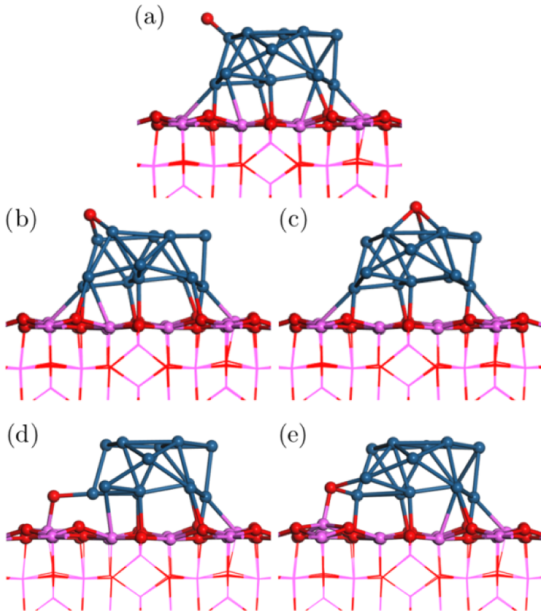

Figure 5. Illustration of top (a), bridge (b), and hollow (c) typical sites with bimetallic (Al, Pt) bridge (d) and hollow (Al, Pt, Pt) sites (e). Platinum atoms are in blue, alumina in pink, and oxygen in red.

DOI: 10.1021/acs.jpcc.8b09204
J. Phys. Chem. C 2018, 122, 26974−26986

oriented to the gas phase (Figure 5a,c). The adsorption energy range does not differ significantly from the second group. These data illustrate the significant promoting effect of the support.

The adsorption energies (in absolute value) at low coverage on Pt(111) are much lower than most of the $Pt_{13}O$ adsorption energies (Table 1 and Supporting Information S6). However, the Pt(111) system with 0.25 ML of oxygen exhibits a similar adsorption energy (−81.3 kcal mol^{-1}) with respect to the particle traditional sites (edges and gas oriented). This tends to indicate that at low oxygen coverage, the main factors determining the reactivity are the nature of the support and its interaction with platinum. Mihai et al.[96] experimentally quantified the heat of adsorption of O_2 on poorly dispersed Pt/Al_2O_3 catalysts (dispersion: 0.12) and obtained values close to −70 kcal mol^{-1} close to single crystal experiments,[97] showing that the support effects becomes substantial only for highly dispersed catalysts, such as the one considered in the present work.

Also, the adsorption energies on the supported cluster are of the same order of magnitude as on nonsupported nano-oxides (n_{Pt} < 13) studied by Schneider et al.[49] At this scale, the bridge adsorption mode is clearly preferred. The case of non-supported Pt_{13} as investigated by Zhang et al.[48] is the exception with two top oxygen atoms, with an adsorption energy close to Pt(111). This supports the idea that the alumina support favors oxygen adsorption.

4.2. Evolution of Adsorption Properties with O Coverage and Cluster Structuration. Higher oxygen coverages were then investigated. Molecular dynamics was used systematically from $Pt_{13}O_2$ to $Pt_{13}O_{32}$ to identify stable configurations (Supporting Information S1). The energetic feature of the most stable systems found is shown in Figure 6.

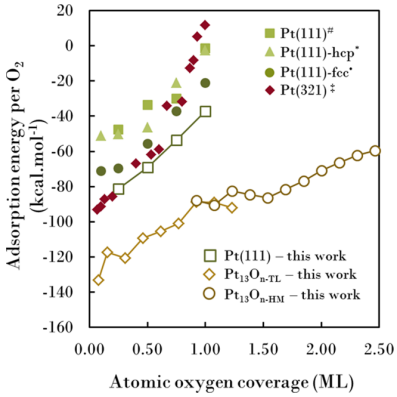

Figure 6. Mean adsorption energies of O_2 according to the oxygen coverage for supported $Pt_{13}O_n$ structures and Pt(111). #Légaré,[20] *•Pang et al.,[21] ‡Schneider and co-workers.[30] For $Pt_{13}O_n$ structures, the monolayer is calculated as the number of oxygen atoms divided by 13, 13 being the number of accessible platinum atoms. Therefore, $Pt_{13}O_{26}$ is considered as a 2 ML structure.

The structure of the systems exhibiting a significant stability domain is depicted in Figure 7, whereas all the discussed structures are reported in the Supporting Information S7.

For all coverages, the bridge adsorption mode is preferred for oxygen on the particle. In the case of bimetallic sites, the bridge mode is still represented, but the bimetallic hollow site (two platinum, one aluminum) dominates. From two oxygen

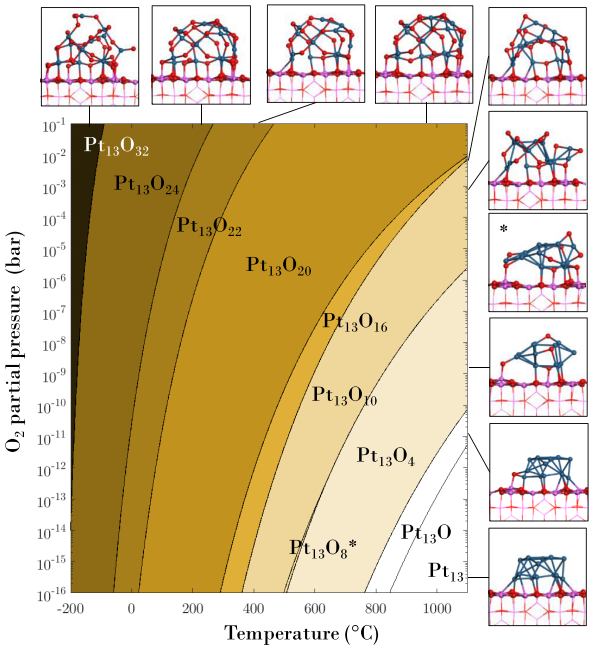

Figure 7. Phase diagram for supported $Pt_{13}O_n$ according to temperature and partial pressure of oxygen. The structures of the systems exhibiting a significant stability domain are also depicted (side views).

atoms adsorbed, the cluster is gradually reconstructed. Two-layers-like structures (noticed TL) are the most stable up to 12 oxygen atoms, deviating, however, strongly from the initial one (without oxygen). Therefore, the 13 platinum atoms become all accessible for n > 10, the single initially occluded atom being displaced in such a way by oxygen that it becomes accessible. At higher oxygen coverages, the particles from $Pt_{13}O_{18}$ to $Pt_{13}O_{26}$ exhibit a fully reconstructed hemispheric shape, referred to hereafter as HM. Within this structure, platinum atoms are tetra- and pentavalent. The oxygen atoms are interspersed between the platinum atoms. This increases the volume of the cluster up to 290% (volume of the platinum polyedra of 84.1 $Å^3$ for Pt_{13} to 201 $Å^3$ for $Pt_{13}O_{24}$). The transition between these two cluster shapes (two layers and hemispheric) appears for intermediate coverages between 14 and 16 oxygen atoms, with a smooth energetic transition (Figure 6).

Finally, the structures at very high coverage, starting from $Pt_{13}O_{26}$, show the disintegration of the hemispheric shape by the adsorption of additional oxygen atoms in the top mode. This comes along with the segregation of a few platinum atoms. Nondissociated O_2 molecules can also be distinguished at high coverages. Although a reconstruction was also observed upon exposure to hydrogen,[41,63] the latter is very different in nature with respect to the one calculated here for oxygen: the bilayer cluster transforms into a cuboctahedron from 20 hydrogen atoms per cluster, with the loss of covalent bonding with the support.

The evolution of the average adsorption energy according to oxygen coverage (Figure 6) decreases (in absolute value) continuously in a quasi-linear way. These values contrast significantly with the ones reported with extended surfaces as Pt(111)[20,21] and Pt(321).[30] The cluster shows a huge capacity of stabilizing oxygen atoms on it.

DOI: 10.1021/acs.jpcc.8b09204
J. Phys. Chem. C 2018, 122, 26974−26986

A (P_{O_2}, T) phase diagram was built, thanks to the entropy and enthalpy obtained with ab initio structures (Figure 7). Contrary to the case of Pt(111) (Supporting Information S6), the diagram for supported Pt_{13} only shows a very small stability domain for zero oxygen coverage. This means that the cluster is always oxidized for realistic oxygen partial pressures in the absence of reducing agent. The diagram is mainly occupied by the high coverage hemispheric structures, having 16−24 oxygen atoms. This is compatible with the experimental observation of poisoning of platinum by oxygen at low dispersion.[98]

Figure 8 summarizes the phase diagrams reported in the literature for a common partial pressure of O_2 of 0.1 bar. The

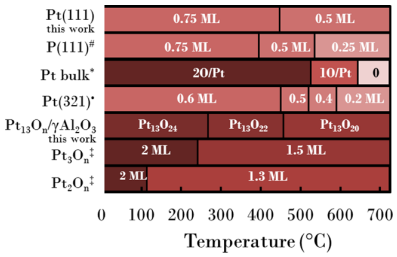

Figure 8. Comparison of platinum−oxygen phase diagrams at P_{O_2} = 0.1 bar according to the nature of the surface. #Légaré,[20] *phase diagram of the bulk platinum in the presence of only O_2 by HSC Chemistry data, •Schneider and co-workers,[30] ‡Schneider and co-workers.[49,50]

capacity of the 13-platinum cluster to hold oxygen is of the same order of magnitude as that of the nonsupported Pt_2 and Pt_3 particles studied by Xu and co-workers.[49,50] This is much higher than the extended surfaces capacity in this condition, but closer to the bulk capacity. The high dispersion, the ductility of the platinum clusters, and the energetics of oxygen adsorption sites are directly related to the capacity of holding such a quantity of oxygen, even at high temperature. This gives an atomistic picture of the origin of the differences between large and small platinum particles for oxygen adsorption and reactions.[18,36,98] Moreover, the stoichiometry of the supported cluster is close to PtO_2 in these pressure conditions, over a large range of temperature.

The platinum/alumina interaction energy is globally strengthening as the oxygen coverage increases (Figure 9a). The opposite trend was noticed on $Pt_{13}H_n$ structures,[63] with an unhooking of the cluster from the support. The impact of the metal/support interaction on the related bond length is not strong (Figure 9b).

Indeed, the average lengths of Pt−Al and Pt−$O_{support}$ bonds do not vary by more than 5%. The single trends that can be seen is the shortening of the Pt−$O_{support}$ bonds from the biplanar to the hemispheric structures, in line with the strengthening of the interaction. Moreover, a substitution of Pt−Al by Al−$O_{cluster}$ bonds occurs with increasing oxygen coverage (Supporting Information S7). Likely, the strongest cluster/support interaction comes from those additional Al−$O_{cluster}$ bonds. The Pt−Pt length increases with oxygen coverage from about 2.8 to 3.4 Å. This represents a 20% rise. The $Pt_{13}O_{14}$ and $Pt_{13}O_{16}$ structures that coexist in the two structure types show that the Pt−Pt bonds are slightly shorter for the hemispheric cluster shape than for the two-layer structure.

To further investigate the impact of oxygen coverage on charge transfer, the Bader partial charges were computed for platinum and oxygen on the cluster (Figure 10). The oxygen

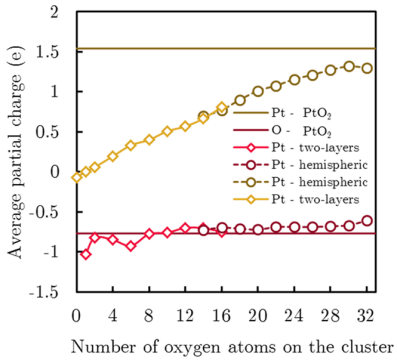

Figure 10. Mean Bader charge per Pt (blue) and cluster O (red) atoms. The cross-shaped dots represent the two-layers structures, whereas full dots stand for hemispheric structures.

charge remains almost constant, with oxygen coverage (between −1 and −0.5) close to the oxygen Bader charge of PtO_2 oxide. However, the charge of platinum increases almost

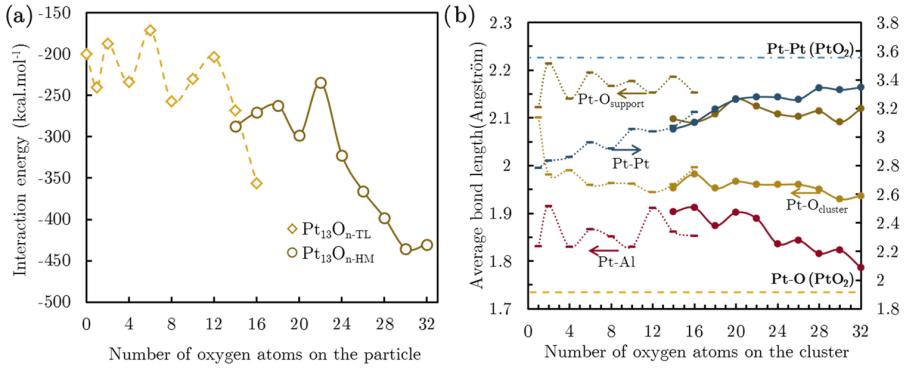

Figure 9. (a) Interaction energy between the alumina support and the oxidized platinum clusters. (b) Average Pt−Pt, Pt−$O_{support}$, and Pt−$O_{cluster}$ bond lengths and minimum Pt−Al length as a function of oxygen coverage. The maximal bond lengths were set to 3.8 Å for Pt−Pt and 2.5 Å for other bonds. Dotted lines corresponds to the two-layer structures, whereas plain lines are hemispheric structures data.

DOI: 10.1021/acs.jpcc.8b09204
J. Phys. Chem. C 2018, 122, 26974−26986

linearly with coverage, starting from a Pt^0 to a 1.2 electron-depleted platinum for very high oxygen coverage, quite close to a kind of PtO_2 charge. The smooth transition noticeable from two layers to hemispheric structures emphasizes the blurred energetic transition discussed previously, showing also that Bader charges are mainly dominated by the stoichiometry of the supported oxide, more than by the morphology. Note that the total charge of the cluster (platinum plus oxygen) remains very close to zero, showing a very weak charge transfer with the support for particles holding oxygen, contrary to what was reported in the presence of hydrogen as adsorbate.[63]

4.3. Activation Energy for the Dissociation of O_2. Potential energy surfaces and transition states for O_2 dissociation were determined on the Pt_{13}/γ-Al_2O_3 model, in comparison with Pt(111). For the supported cluster, three coverages were investigated: (1) the dissociation of O_2 on a reduced particle (from 0 to 2 oxygen atoms per cluster), (2) with an intermediate coverage on a two-layer cluster structure (from 8 to 10 oxygen atoms per cluster), and (3) on a high oxygen coverage cluster with an hemispheric shape (from 22 to 24 oxygen atoms per cluster). For Pt(111), two energetic pathways were investigated: the dissociation of O_2 on a reduced surface and another one with an initial 0.5 ML atomic oxygen coverage. On the later structure, the dissociation leads to a 1 ML oxygen coverage. In all cases, this evaluation was performed using the most stable final state. The energy paths are summarized in Figure 11, with the key structures

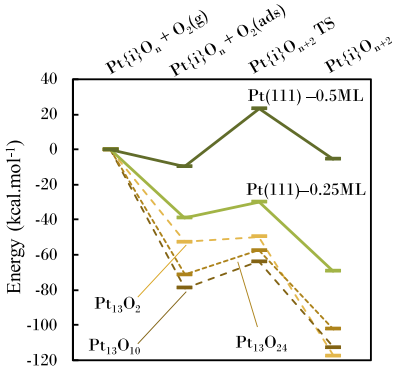

Figure 11. Dissociation barriers from initial state $Pt_{13}O_n$ to $Pt_{13}O_{n+2}$ and $Pt(111)O_n$ to $Pt(111)O_{n+2}$. The energies are displayed relatively to each initial state energy.

(including transition structures) shown in the Supporting Information S8. The latter corresponds to the O−O bond elongation. Adsorption of a nondissociated O_2 is energetically favored, more strongly on the clusters than on Pt(111). Notably, on Pt(111), the molecular adsorption of O_2 is more favorable on the reduced surface, whereas the reverse trend is observed for the cluster, with more negative energies in the case of the oxidized cluster.

The dissociation barriers from adsorbed O_2 (forward and backward) are given in Table 2. Fu et al. report a similar behavior with a O−O bond scission with a 8.8 kcal mol^{-1} barrier on a reduced surface of Pt(111).[56] A 8.3 kcal mol^{-1} barrier is calculated for the low coverage dissociation on Pt(111). It reaches 32.5 kcal mol^{-1} for the medium coverage. Consequently, the atomic oxygen coverage has a significant inhibiting effect on O_2 dissociation for Pt(111). For the supported Pt_{13} cluster, a 3 kcal mol^{-1} barrier for the reduced particle is obtained, whereas the one with a medium coverage is about 15 kcal mol^{-1}, despite the same two-layer structure. On the contrary, no significant influence of the cluster structuration (HM versus TL) is noticed as the activation energy found for $Pt_{13}O_{24}$ formation is almost equivalent to that of $Pt_{13}O_{10}$. Note that Zhang and co-workers[48] found an activation energy of 10 kcal mol^{-1} on a nonsupported Pt_{13}-reduced particle, within the interval we find here.

To conclude, the ab initio investigations of supported $Pt_{13}O_n$ clusters reveal a very strong affinity of the catalytic system for oxygen, leading to highly oxidized stoichiometry, whose dependence is elucidated as a function of the temperature and O_2 pressure. The metal/support interaction is strengthened upon oxidation, thanks to platinum−oxygen−aluminum bridges. A reconstruction takes place from a biplanar-like morphology at low coverage to hemispherical shapes at high coverage. Dissociation barriers of O_2 were also determined and significantly depend on the oxygen coverage. It is now worth analyzing the macroscopic consequences of such microscopic features, which is done thanks to multiscale kinetic modeling.

5. KINETIC MODELING OF O_2-TPD

Detailed kinetic models were developed to deduce the expected TPD profile from ab initio calculations (Supporting Information S9), together with the definition of the surface species present throughout the TPD. The kinetic model analysis is performed on several key parameters to evaluate its ability to simulate the TPD. Earlier ab initio calculations emphasize on the close energy structures for specific oxygen coverages. The impact of the scheme structuration on the O_2 release has been benchmarked. This allows to evaluate the scheme complexity level toward the experimental data. Considering a scheme that takes into account all the structures, sensitivity analysis and reaction path analyses have been performed. Therefore, both key structures and reactions are identified.

5.1. Impact of the Dispersion on O_2-TPD. The most stable structures determined by ab initio calculations for each oxygen coverage were used to build the present kinetic mechanism. To represent the complex transition between the two-layer (TL) and hemispheric (HM) structures, two structures were considered for $Pt_{13}O_{14}$ and $Pt_{13}O_{16}$ with their

Table 2. Dissociation and Association Barriers for O_2 Dissociation on Pt(111) and $Pt_{13}O_n$ Cluster

reaction	dissociation barrier (kcal mol^{-1})	association barrier (kcal mol^{-1})
$Pt(111) + O_2(g) \rightarrow Pt(111)$-0.25 ML	8.3	67.7
$Pt(111)$-0.25 ML $+ O_2(g) \rightarrow Pt(111)$-0.5 ML	32.5	48.9
$Pt_{13} + O_2(g) \rightarrow Pt_{13}O_2$	3.0	47.8
$Pt_{13}O_8 + O_2(g) \rightarrow Pt_{13}O_{10}$	15.1	39.2
$Pt_{13}O_{22} + O_2(g) \rightarrow Pt_{13}O_{24}$	13.8	45.0

DOI: 10.1021/acs.jpcc.8b09204
J. Phys. Chem. C 2018, 122, 26974−26986

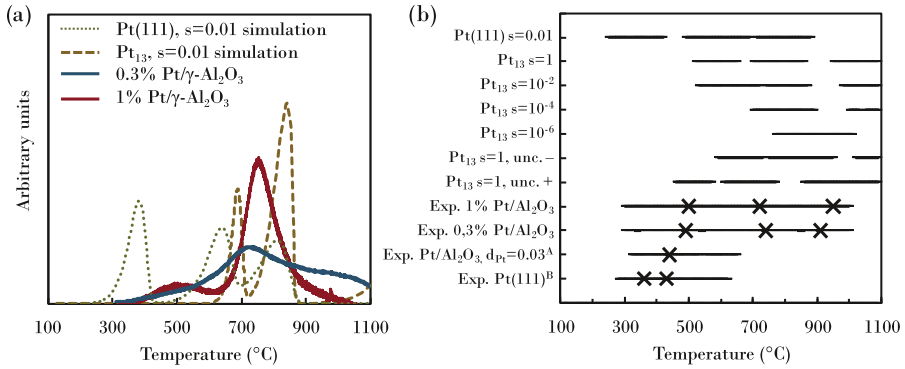

Figure 12. (a) Predicted O_2 concentration profile during O_2-TPD with Pt(111) and Pt_{13}, with TPD experiments on highly dispersed Pt/γ-Al_2O_3. (b) Impact of sticking coefficient and a typical error (±3.6 kcal mol^{-1} for enthalpies and ±3.6 cal mol^{-1} K^{-1} for entropies, see text) on Pt_{13} kinetic model with a 5 °C min^{-1} temperature ramp and starting with the $Pt_{13}O_{20}$ structure. The O_2-TPD experiments of [A]Olsson et al.[95] and [B]Parker et al.[93] are also reported. The lines represent the range of occurrence of O_2 release and the crosses the associated rate-of-desorption maxima.

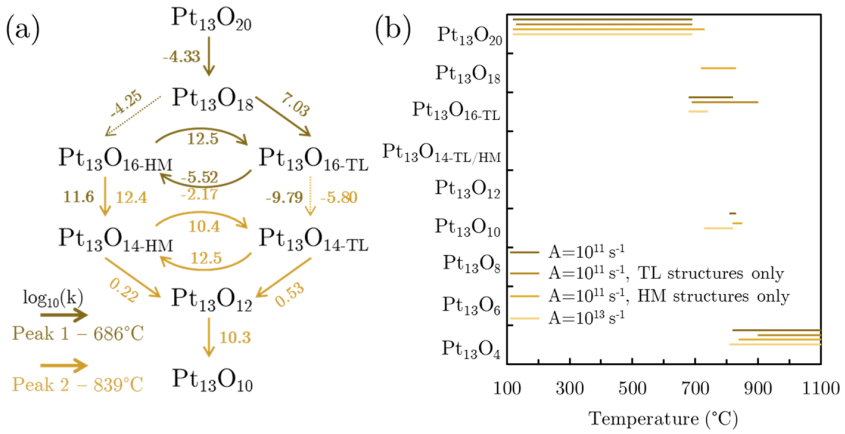

Figure 13. (a) Logarithm of the rate constants (in s^{-1}) at the peak temperature for $Pt_{13}O_n$ kinetic mechanism. The sticking coefficient of O_2 is 10^{-2}. (b) Predominant surface species during TPD experiments with distinct scheme structure. The impact of the pre-exponential factor of the two surface reaction A is studied as well as the two paths involving $Pt_{13}O_{n\text{-TL}}$ or $Pt_{13}O_{n\text{-HM}}$ independently. The sticking coefficient of O_2 is 10^{-2}. The reference scheme is the darker one.

own kinetic parameters. To correctly depict this transition, two reversible surface reactions were implemented to connect one structure to the other. The activation energies come from ab initio data, the pre-exponential factors were set to 10^{11} s^{-1} as recommended for nonrotating and nonmobile adsorbate by Dumesic et al.[99]

An important parameter likely affected by Pt dispersion is the sticking coefficient (eq 6). Ertl et al. investigated it on Pt(111) in vacuum conditions.[22] They found that it depends on the collision angle with the surface, the oxygen coverage, and the temperature and is of the order of 10^{-2}. Therefore, several coefficients were attempted in this work for the Pt_{13} mechanism, starting from a trial value of 10^{-2}.

Figure 12 shows the simulations of the O_2-TPD experiment with Pt(111) and Pt_{13} kinetic models with a sticking coefficient of 10^{-2} for all the reactions. The Pt_{13} simulation exhibits two successive desorption peaks at 686 and 839 °C, corresponding to the transition from $Pt_{13}O_{20}$ to $Pt_{13}O_{16\text{-TL}}$ and then to $Pt_{13}O_4$, respectively. These peaks lie in the temperature ranges of the main experimental TPD peak, above 700 °C. In the case of the Pt(111) simulation, three peaks are obtained (at 384, 639, and 814 °C for $s = 10^{-2}$, corresponding to 0.75 ML → 0.50 ML → 0.25 ML → 0 ML, respectively). The desorption is here centered around 600 °C.

Experimental TPD of Olsson et al.[95] (poorly dispersed supported catalysts) and Parker et al.[93] (Pt(111)) show, respectively, one and three peaks in the same temperature range from 300 to 600 °C. The temperature ramp applied in their studies are quite different (40 °C min^{-1} and 8 °C s^{-1} respectively) and may impact the O_2-TPD shape. In contrast, the O_2 adsorption kinetic parameters of Deutschmann[100] (version of Nov 1995 with duplicated adsorption reaction) were implemented in our own kinetic model, which leads to a broad signal from 100 to 1100 °C with a simulated ramp of 5 °C min^{-1}.

The sticking coefficient is typically measured at very low pressure (<0.1 atm), which is not representative of the thermodynamic conditions of the TPD experiment. Several studies[22,90,91] put forward that the O_2 sticking coefficient for Pt(111) surface lies around 10^{-2}. For Pt(111)-stepped surfaces,[101,102] the coefficients were higher and around 10^{-1}, but the sites were quickly saturated. Considering the peculiar structure of the Pt_{13} cluster, we varied the sticking coefficient of O_2 from 1 to 10^{-6}. Even though the sticking coefficient is expected to decrease with θ_O, it was assumed to be

DOI: 10.1021/acs.jpcc.8b09204
J. Phys. Chem. C 2018, 122, 26974−26986

independent of oxygen coverage for the sake of simplifying the analysis of its impact on desorption. According to the present model, the two O_2 peaks start to merge for sticking probabilities lower than the threshold value of 10^{-2} (Figure 12b and S14). A slight shift toward higher temperatures is observed for the third desorption process.

The estimation of enthalpies and entropies from ab initio calculations can also lead to an error for methodological reasons. To estimate the consequences of typical errors, we built two kinetic models that lower or enhance the reactivity. The sticking coefficient of O_2 was set to 1. The model that enhances the kinetic (named Pt_{13} unc. + in Figure 12b) is built so that 3.6 cal mol^{-1} K^{-1} are added to each $\Delta_r S_{desorption}$ and 3.6 kcal mol^{-1} are removed to $E_{dissociation}$ and $\Delta_r H_{desorption}$. In that case, a 60 °C peak shift is noticed. The Pt_{13} unc. − model displays two merged peaks at low temperature and a 70 °C shift to higher temperatures.

From our analyses, one can conclude that all desorptions are simulated above 500 °C with the Pt_{13} model, in line with the highest temperature peaks recorded experimentally for both 1 and 0.3% Pt/γ-Al_2O_3 ultradispersed catalysts. The lower temperature peaks are better explained by our Pt(111) ab initio kinetic model, suggesting that the biggest particles are at the origin of these peaks. Accordingly, they were shown to be more abundant on the 1% Pt/γ-Al_2O_3 catalyst (Figure 2). The Pt_{13} model remains too discrete with respect to the experiments, with two sharp peaks (686 and 839 °C) surrounding the experimental main large peak (757−710 °C, depending on the sample). This suggests that considering a single cluster size, initial morphology and support orientation are an oversimplified description of the system. However, the main trends are captured, which is clearly impossible with an ideal surface model such as Pt(111).

5.2. Reaction Paths Analyses. As the current model is able to reproduce TPD experiment correctly at high temperatures, we may perform path analyses to interpret the model behavior at high temperatures. The logarithm of the rate constants taken at the temperature of the peaks are reported in Figure 13a. It shows that the preferential path goes through $Pt_{13}O_{16\text{-TL}}$, which is the predominant structure between 630 and 810 °C. The rate constants are sufficiently high to desorb more oxygen via the reaction between $Pt_{13}O_{16\text{-HM}}$ and $Pt_{13}O_{14\text{-HM}}$. The preferred path engages then both $Pt_{13}O_{14\text{-TL}}$ and $Pt_{13}O_{14\text{-HM}}$ to $Pt_{13}O_{12}$.

The pre-exponential parameters of $Pt_{13}O_{22}$ reduction to $Pt_{13}O_{20}$ appear by far as the most important ones for O_2 concentration prediction, the sensitivity being 40 times higher than that of the $Pt_{13}O_{18}$ to $Pt_{13}O_{16}$-HM reaction. This sensitivity is however significant only between 310 and 380 °C, before the first desorption peak occurs. This suggests that some $Pt_{13}O_{22}$ may appear at low temperature and desorbs at lower temperature than the first observed peak.

To evaluate the impact of the four structures for n = 14 and 16, the TPD was predicted with only TL structures or HM structures using two distinct schemes. The predominant species are displayed in Figure 13b, as a function of the temperature. First and foremost, the major species remains $Pt_{13}O_{20}$ up to the same temperature for the common scheme and the TL one. The desorption of O_2 from this species is predicted to occur at higher temperature for HM model than for TL model. Whereas the TM model proceeds mainly through $Pt_{13}O_{16\text{-TL}}$, the HM scheme predicts a direct desorption from $Pt_{13}O_{18}$ to $Pt_{13}O_{10}$. Moreover, the pre-exponential factor set for the surface reactions has a very modest impact on O_2 release and does not induce any variation in the scheme path.

Finally, one may compare the stability domains given by the kinetic model (Figure 13b) and from the ab initio thermodynamic diagram (Figure 7). Trying to depict the species appearing in the course of the TPD by a single O_2 partial pressure and by an equilibrium situation is not possible, as we should have a large kinetic stability domain for $Pt_{13}O_8$ in any case, before reaching $Pt_{13}O_4$. This shows that kinetic limitations play a strong role in TPD, which cannot be described by a simple thermodynamic diagram.

Considering the temperature ranges of O_2 desorption, the multiscale approach, which relies on ab initio calculations for microkinetic model development, provides a consistent model. In addition, the kinetic analyses offers an unrivaled mean to interpret the features of the experimental O_2-TPD. It highlights the effect of complex systems involving different cluster geometries, which tend to be more realistic. In addition, the kinetic analysis demonstrates that both cluster morphologies (two-layer and hemispherical) must be considered for O_2 desorption.

6. CONCLUSIONS

In the present work, we have presented a multiscale approach applied to oxygen adsorption on highly dispersed Pt/γ-Al_2O_3, combining TPD experiments, ab initio, and kinetic modeling. High-temperature desorption was observed experimentally, suggesting that much stronger interactions exist between oxygen and Pt_{13} clusters than for extended surfaces. The ab initio electronic calculations of a 13-platinum cluster supported on alumina shows that the support is involved for the most stable adsorption sites. A morphology change is observed according to oxygen coverage, with a low coverage structure characterized by two parallel layers of platinum and an hemispherical shape at high coverage. Ab initio thermodynamic data allow to build a phase diagram that shows a highly oxidized cluster for accessible O_2 pressure and temperature. The same study was applied to the Pt(111) surface. Kinetic schemes were then set up to simulate TPD experiments using Pt_{13} and Pt(111) ab initio simulated thermokinetic parameters. Despite some uncertainties on sticking coefficient and desorption free energy barriers, the two models suggest that the experimental low temperature desorption is in agreement with some peak of the Pt(111) simulated TPD, characteristic of large particle with regular facets, whereas high-temperature desorption is clearly the contribution of small platinum particles.

Finally, this work highlights the reactivity of highly dispersed platinum supported on alumina. Several computed thermochemical data such as the heat of adsorption and the achievable oxygen coverage thoroughly differ from well-known extended surfaces. The temperature-programmed desorption of O_2 and the related kinetic simulations demonstrate similar desorption temperature ranges that again consolidate the approach of coupling the experimental and the modeling work. The model established herein could be implemented in the future for highly dispersed platinum catalysis mechanism in oxidant media, such as oxidation of carbon monoxide into CO_2. Some in-depth work would be needed regarding kinetic parameters such as the sticking probability. Also, it is shown that special attention has to be given to account for the structural dimension of modeled systems and its translation in the kinetic

DOI: 10.1021/acs.jpcc.8b09204
J. Phys. Chem. C 2018, 122, 26974−26986

scheme. Yet, complex ab initio models, including a support, an anisotropic catalyst structure, and a large oxygen coverage range, among others, are herein shown to be relevant when integrated in a kinetic scheme according to the conducted O_2-TPD experiments.

■ ASSOCIATED CONTENT

Supporting Information

The Supporting Information is available free of charge on the ACS Publications website at DOI: 10.1021/acs.jpcc.8b09204.

Illustration of a typical velocity-scaled MD run with cluster reconstruction; estimation of the Gibbs free energy of adsorption; X-ray fluorescence for the two catalysts; optimization of the TPD protocol; deconvolution of the TPD profiles; dissociative adsorption of O_2 on Pt(111) investigated by ab initio calculations; most stable structures found for the supported $Pt_{13}O_n$ system from ab initio calculations; transition structures for the dissociation of O_2; kinetic parameters for the $Pt_{13}O_n$ model and Pt(111) model (PDF)

■ AUTHOR INFORMATION

Corresponding Author

*E-mail: celine.chizallet@ifpen.fr.

ORCID

Céline Chizallet: 0000-0001-5140-8397

Notes

The authors declare no competing financial interest.

■ ACKNOWLEDGMENTS

The authors thank C. Guegan and F. Diehl (Catalysis and Separation Division, IFP Energies nouvelles) for providing the Pt/γ-Al_2O_3 catalysts and O. Gardoll for help in the TPD experiments undertook at UCCS laboratory at Villeneuve d'Ascq, France. All ab initio calculations were performed on the ENER110 supercomputer at IFP Energies nouvelles.

■ REFERENCES

(1) Bell, A. T. The Impact of Nanoscience on Heterogeneous Catalysis. *Science* **2003**, *299*, 1688−1691.

(2) Gates, B. C. Supported Metal Clusters: Synthesis, Structure, and Catalysis. *Chem. Rev.* **1995**, *95*, 511−522.

(3) Chen, A.; Holt-Hindle, P. Platinum-Based Nanostructured Materials: Synthesis, Properties, and Applications. *Chem. Rev.* **2010**, *110*, 3767−3804.

(4) Sun, G.; Sautet, P. Metastable Structures in Cluster Catalysis from First-Principles: Structural Ensemble in Reaction Conditions and Metastability Triggered Reactivity. *J. Am. Chem. Soc.* **2018**, *140*, 2812−2820.

(5) Sattler, J. J.; Ruiz-Martinez, J.; Santillan-Jimenez, E.; Weckhuysen, B. M. Catalytic Dehydrogenation of Light Alkanes on Metals and Metal Oxides. *Chem. Rev.* **2014**, *114*, 10613−10653.

(6) Avenier, P.; Bazer-Bachi, D.; Bazer-Bachi, F.; Chizallet, C.; Deleau, F.; Diehl, F.; Gornay, J.; Lemaire, É.; Moizan-Basle, V.; Plais, C.; et al. Catalytic Reforming: Methodology and Process Development for a Constant Optimisation and Performance Enhancement. *Oil Gas Sci. Technol.* **2016**, *71*, 41−59.

(7) Burch, R. Knowledge and Know-How in Emission Control for Mobile Applications. *Catal. Rev.* **2004**, *46*, 271−334.

(8) Sinfelt, J. H. Catalytic Reforming. In *Handbook of Heterogeneous Catalysis*; Ertl, G., Knözinger, E., Weitkamp, J., Eds.; Wiley: Weinheim, 1997; pp 1939−1955.

(9) Russell, A.; Epling, W. S. Diesel Oxidation Catalysts. *Catal. Rev.* **2011**, *53*, 337−423.

(10) Morozan, A.; Jousselme, B.; Palacin, S. Low-Platinum and Platinum-Free Catalysts for the Oxygen Reduction Reaction at Fuel Cell Cathodes. *Energy Environ. Sci.* **2011**, *4*, 1238−1254.

(11) Gasteiger, H. A.; Kocha, S. S.; Sompalli, B.; Wagner, F. T. Activity Benchmarks and Requirements for Pt, Pt-Alloy, and non-Pt Oxygen Reduction Catalysts for PEMFCs. *Appl. Catal., B* **2005**, *56*, 9−35.

(12) Lykhach, Y.; Bruix, A.; Fabris, S.; Potin, V.; Matolinova, I.; Matolin, V.; Libuda, J.; Neyman, K. M. Oxide-Based Nanomaterials for Fuel Cell Catalysis: the Interplay between Supported Single Pt Atoms and Particles. *Catal. Sci. Technol.* **2017**, *7*, 4315−4345.

(13) Marković, N. M.; Schmidt, T. J.; Stamenković, V.; Ross, P. N. Oxygen Reduction Reaction on Pt and Pt Bimetallic Surfaces: A Selective Review. *Fuel Cells* **2001**, *1*, 105−116.

(14) European Commission. *Critical Raw Materials for the EU*, http://ec.europa.eu/growth/sectors/raw-materials/specific-interest/critical_fr (accessed Nov 12, 2018).

(15) Roduner, E. Size Matters: why Nanomaterials are Different. *Chem. Soc. Rev.* **2006**, *35*, 583−592.

(16) Roldan Cuenya, B.; Behafarid, F. Nanocatalysis: size- and shape-dependent chemisorption and catalytic reactivity. *Surf. Sci. Rep.* **2015**, *70*, 135−187.

(17) Zhai, H.; Alexandrova, A. N. Fluxionality of Catalytic Clusters: When It Matters and How to Address It. *ACS Catal.* **2017**, *7*, 1905−1911.

(18) García-Diéguez, M.; Chin, Y.-H.; Iglesia, E. Catalytic Reactions of Dioxygen with Ethane and Methane on Platinum Clusters: Mechanistic Connections, Site Requirements, and Consequences of Chemisorbed Oxygen. *J. Catal.* **2012**, *285*, 260−272.

(19) Weaver, J. F.; Chen, J.-J.; Gerrard, A. L. Oxidation of Pt(111) by Gas-Phase Oxygen Atoms. *Surf. Sci.* **2005**, *592*, 83−103.

(20) Légaré, P. Interaction of Oxygen with the Pt(111) Surface in Wide Conditions Range. A DFT-Based Thermodynamical Simulation. *Surf. Sci.* **2005**, *580*, 137−144.

(21) Pang, Q.; Zhang, Y.; Zhang, J.-M.; Xu, K.-W. Structural and Electronic Properties of Atomic Oxygen Adsorption on Pt(111): A Density-Functional Theory Study. *Appl. Surf. Sci.* **2011**, *257*, 3047−3054.

(22) Campbell, C. T.; Ertl, G.; Kuipers, H.; Segner, J. A Molecular Beam Study of the Adsorption and Desorption of Oxygen from a Pt(111) Surface. *Surf. Sci.* **1981**, *107*, 220−236.

(23) Elg, A.-P.; Eisert, F.; Rosén, A. The Temperature Dependence of the Initial Sticking Probability of Oxygen on Pt(111) Probed with Second Harmonic Generation. *Surf. Sci.* **1997**, *382*, 57−66.

(24) Hwang, C.-P.; Yeh, C.-T. Platinum-Oxide Species Formed by Oxidation of Platinum Crystallites Supported on Alumina. *J. Mol. Catal. A: Chem.* **1996**, *112*, 295−302.

(25) Salmerón, M.; Brewer, L.; Somorjai, G. A. The Structure and Stability of Surface Platinum Oxide and of Oxides of Other Noble Metals. *Surf. Sci.* **1981**, *112*, 207−228.

(26) Fantauzzi, D.; Mueller, J. E.; Sabo, L.; van Duin, A. C.; Jacob, T. Surface Buckling and Subsurface Oxygen: Atomistic Insights into the Surface Oxidation of Pt(111). *ChemPhysChem* **2015**, *16*, 2797−2802.

(27) Krasnikov, S. A.; Murphy, S.; Berdunov, N.; McCoy, A. P.; Radican, K.; Shvets, I. V. Self-Limited Growth of Triangular PtO_2 Nanoclusters on the Pt(111) Surface. *Nanotechnology* **2010**, *21*, No. 335301.

(28) Devarajan, S. P.; Hinojosa, J. A.; Weaver, J. F. STM Study of High-Coverage Structures of Atomic Oxygen on Pt(111): p(2×1) and Pt Oxide Chain Structures. *Surf. Sci.* **2008**, *602*, 3116−3124.

(29) van Spronsen, M. A.; Frenken, J. W. M.; Groot, I. M. N. Observing the Oxidation of Platinum. *Nat. Commun.* **2017**, *8*, No. 429.

(30) Bray, J. M.; Smith, J. L.; Schneider, W. F. Coverage-Dependent Adsorption at a Low Symmetry Surface: DFT and Statistical Analysis of Oxygen Chemistry on Kinked Pt(321). *Top. Catal.* **2014**, *57*, 89−105.

DOI: 10.1021/acs.jpcc.8b09204
J. Phys. Chem. C 2018, 122, 26974−26986

(31) Jenkins, S. J.; Petersen, M. A.; King, D. A. Comparative theory of missing-row reconstructions: Pt{110}, Pt{211} and Pt{311}. *Surf. Sci.* **2001**, *494*, 159−165.
(32) Carlsson, P.-A.; Mollner, S.; Arnby, K.; Skoglundh, M. Effect of Periodic Operation on the Low-Temperature Activity for Propane Oxidation over Pt/Al_2O_3 catalysts. *Chem. Eng. Sci.* **2004**, *59*, 4313−4323.
(33) Yazawa, Y.; Yoshida, H.; Hattori, T. The Support Effect on Platinum Catalyst under Oxidizing Atmosphere: Improvement in the Oxidation-Resistance of Platinum by the Electrophilic Property of Support Materials. *Appl. Catal., A* **2002**, *237*, 139−148.
(34) Wang, C.-B.; Yeh, C.-T. Effects of Particle Size on the Progressive Oxidation of Nanometer Platinum by Dioxygen. *J. Catal.* **1998**, *178*, 450−456.
(35) Shelimov, B.; Lambert, J.-F.; Che, M.; Didillon, B. Application of NMR to Interfacial Coordination Chemistry: A ^{195}Pt NMR Study of the Interaction of Hexachloroplatinic Acid Aqueous Solutions with Alumina. *J. Am. Chem. Soc.* **1999**, *121*, 545−556.
(36) Gruber, H. L. Chemisorption Studies on Supported Platinum. *J. Phys. Chem.* **1962**, *66*, 48−54.
(37) O'Rear, D. J.; Löffler, D. G.; Boudart, M. Stoichiometry of the Titration by Dihydrogen of Oxygen Adsorbed on Platinum. *J. Catal.* **1990**, *121*, 131−140.
(38) Vannice, M. A.; Benson, J. E.; Boudart, M. Determination of Surface Area by Chemisorption: Unsupported Platinum. *J. Catal.* **1970**, *16*, 348−356.
(39) Boudart, M. Catalysis by Supported Metals. *Adv. Catal.* **1969**, *20*, 153−166.
(40) Euzen, P.; Raybaud, P.; Krokidis, X.; Toulhoat, H.; Loarer, J. L.; Jolivet, J.-P.; Froidefond, C. Alumina. In *Handbook of Porous Solids*; Schüth, F., Sing, K. S. W., Weitkamp, J., Eds.; Wiley-VCH: Weinheim, 2002.
(41) Gorczyca, A.; Moizan, V.; Chizallet, C.; Proux, O.; Del Net, W.; Lahera, E.; Hazemann, J. L.; Raybaud, P.; Joly, Y. Monitoring Morphology and Hydrogen Coverage of Nanometric Pt/Gamma-Al_2O_3 Particles by in situ HERFD−XANES and Quantum Simulations. *Angew. Chem., Int. Ed.* **2014**, *53*, 12426−12429.
(42) Kwak, J. H.; Hu, J.; Mei, D.; Yi, C. W.; Kim, D. H.; Peden, C. H. F.; Allard, L. F.; Szanyi, J. Coordinatively Unsaturated Al^{3+} Centers as Binding Sites for Active Catalyst Phases of Platinum on Gamma-Al_2O_3. *Science* **2009**, *325*, 1670−1673.
(43) Nellist, P. D.; Pennycook, S. J. Direct Imaging of the Atomic Configuration of Ultradispersed Catalysts. *Science* **1996**, *274*, 413−415.
(44) Sinkler, W.; Sanchez, S. I.; Bradley, S. A.; Wen, J.; Mishra, B.; Kelly, S. D.; Bare, S. R. Aberration-Corrected Transmission Electron Microscopy and In Situ XAFS Structural Characterization of Pt/γ-Al_2O_3 Nanoparticles. *ChemCatChem* **2015**, *7*, 3779−3787.
(45) Raybaud, P.; Chizallet, C.; Mager-Maury, C.; Digne, M.; Toulhoat, H.; Sautet, P. From Gamma-Alumina to Supported Platinum Nanoclusters in Reforming Conditions: 10 years of DFT Modeling and Beyond. *J. Catal.* **2013**, *308*, 328−340.
(46) Chizallet, C.; Raybaud, P. Density Functional Theory Simulations of Complex Catalytic Materials in Reactive Environments: Beyond the Ideal Surface at Low Coverage. *Catal. Sci. Technol.* **2014**, *4*, 2797−2813.
(47) Trinchero, A.; Klacar, S.; Paz-Borbón, L. O.; Hellman, A.; Grönbeck, H. Oxidation at the Subnanometer Scale. *J. Phys. Chem. C* **2015**, *119*, 10797−10803.
(48) Zhang, W.; Sumer, A.; Jellinek, J.; Cheng, D. Morphology Tailoring of Pt Nanocatalysts for the Oxygen Reduction Reaction: The Paradigm of Pt_{13}. *ChemNanoMat* **2015**, *1*, 482−488.
(49) Xu, Y.; Shelton, W. A.; Schneider, W. F. Effect of Particle Size on the Oxidizability of Platinum Clusters. *J. Phys. Chem. A* **2006**, *110*, 5839−5846.
(50) Xu, Y.; Shelton, W. A.; Schneider, W. F. Thermodynamic Equilibrium Compositions, Structures, and Reaction Energies of Pt_xO_y (x = 1−3) Clusters Predicted from First Principles. *J. Phys. Chem. B* **2006**, *110*, 16591−16599.
(51) Jennings, P. C.; Aleksandrov, H. A.; Neyman, K. M.; Johnston, R. L. A DFT Study of Oxygen Dissociation on Platinum based Nanoparticles. *Nanoscale* **2014**, *6*, 1153−1165.
(52) Hu, C. H.; Chizallet, C.; Toulhoat, H.; Raybaud, P. Structural, Energetic, and Electronic Trends in Low-Dimensional Late-Transition-Metal Systems. *Phys. Rev. B* **2009**, *79*, No. 195416.
(53) Hu, C. H.; Chizallet, C.; Mager-Maury, C.; Corral Valero, M.; Sautet, P.; Toulhoat, H.; Raybaud, P. Modulation of Catalyst Particle Structure upon Support Hydroxylation: *Ab Initio* Insights for Pd_{13} and Pt_{13} / Gamma-Al_2O_3. *J. Catal.* **2010**, *274*, 99−110.
(54) Li, L.; Larsen, A. H.; Romero, N. A.; Morozov, V. A.; Glinsvad, C.; Abild-Pedersen, F.; Greeley, J.; Jacobsen, K. W.; Norskov, J. K. Investigation of Catalytic Finite-Size-Effects of Platinum Metal Clusters. *J. Phys. Chem. Lett.* **2013**, *4*, 222−226.
(55) Holby, E. F.; Greeley, J.; Morgan, D. Thermodynamics and Hysteresis of Oxide Formation and Removal on Platinum (111) Surfaces. *J. Phys. Chem. C* **2012**, *116*, 9942−9946.
(56) Fu, Q.; Yang, J.; Luo, Y. A First Principles Study on the Dissociation and Rotation Processes of a Single O_2 Molecule on the Pt(111) Surface. *J. Phys. Chem. C* **2011**, *115*, 6864−6869.
(57) Watwe, R. M.; Cortright, R. D.; Mavrikakis, M.; Norskov, J. K.; Dumesic, J. A. Density Functional Theory Studies of the Adsorption of Ethylene and Oxygen on Pt(111) and Pt_3Sn(111). *J. Chem. Phys.* **2001**, *114*, 4663−4668.
(58) Bray, J. M.; Skavdahl, I. J.; McEwen, J. S.; Schneider, W. F. First-Principles Reaction Site Model for Coverage-Sensitive Surface Reactions: Pt(111)−O Temperature Programmed Desorption. *Surf. Sci.* **2014**, *622*, L1−L6.
(59) Zhu, T.; Sun, S.-G.; van Santen, R. A.; Hensen, E. J. M. Reconstruction of Clean and Oxygen-Covered Pt(110) Surfaces. *J. Phys. Chem. C* **2013**, *117*, 11251−11257.
(60) Liu, D. J.; Evans, J. W. Interactions Between Oxygen Atoms on Pt(100): Implications for Ordering during Chemisorption and Catalysis. *ChemPhysChem* **2010**, *11*, 2174−2181.
(61) Nguyen, T. Q.; Escaño, M. C. S.; Nakanishi, H.; Kasai, H.; Maekawa, H.; Osumi, K.; Sato, K. DFT+U Study on the Oxygen Adsorption and Dissociation on CeO_2-Supported Platinum Cluster. *Appl. Surf. Sci.* **2014**, *288*, 244−250.
(62) Wang, X.; van Bokhoven, J. A.; Palagin, D. Ostwald Ripening versus Single Atom Trapping: towards Understanding Platinum Particle Sintering. *Phys. Chem. Chem. Phys.* **2017**, *19*, 30513−30519.
(63) Mager-Maury, C.; Bonnard, G.; Chizallet, C.; Sautet, P.; Raybaud, P. H_2-Induced Reconstruction of Supported Pt Clusters: Metal−Support Interaction versus Surface Hydride. *ChemCatChem* **2011**, *3*, 200−207.
(64) Saeys, M.; Reyniers, M.-F.; Thybaut, J. W.; Neurock, M.; Marin, G. B. First-Principles Based Kinetic Model for the Hydrogenation of Toluene. *J. Catal.* **2005**, *236*, 129−138.
(65) Salciccioli, M.; Stamatakis, M.; Caratzoulas, S.; Vlachos, D. G. A Review of Multiscale Modeling of Metal-Catalyzed Reactions: Mechanism Development for Complexity and Emergent Behavior. *Chem. Eng. Sci.* **2011**, *66*, 4319−4355.
(66) Reuter, K. Ab Initio Thermodynamics and First-Principles Microkinetics for Surface Catalysis. *Catal. Lett.* **2016**, *146*, 541−563.
(67) Sabbe, M. K.; Canduela-Rodriguez, G.; Joly, J.-F.; Reyniers, M.-F.; Marin, G. B. Ab Initio Coverage-Dependent Microkinetic Modeling of Benzene Hydrogenation on Pd(111). *Catal. Sci. Technol.* **2017**, *7*, 5267−5283.
(68) John, M.; Alexopoulos, K.; Reyniers, M.-F.; Marin, G. B. Effect of Zeolite Confinement on the Conversion of 1-Butanol to Butene Isomers: Mechanistic Insights from DFT Based Microkinetic Modelling. *Catal. Sci. Technol.* **2017**, *7*, 2978−2997.
(69) Larmier, K.; Chizallet, C.; Maury, S.; Cadran, N.; Abboud, J.; Lamic-Humblot, A. F.; Marceau, E.; Lauron-Pernot, H. Isopropanol Dehydration on Amorphous Silica-Alumina: Synergy of Bronsted and Lewis Acidities at Pseudo-Bridging Silanols. *Angew. Chem., Int. Ed.* **2017**, *56*, 230−234.
(70) Larmier, K.; Nicolle, A.; Chizallet, C.; Cadran, N.; Maury, S.; Lamic-Humblot, A.-F.; Marceau, E.; Lauron-Pernot, H. Influence of

DOI: 10.1021/acs.jpcc.8b09204
J. Phys. Chem. C 2018, 122, 26974−26986

Coadsorbed Water and Alcohol Molecules on Isopropyl Alcohol Dehydration on γ-Alumina: Multiscale Modeling of Experimental Kinetic Profile. *ACS Catal.* **2016**, *6*, 1905−1920.
(71) Rankovic, N.; Chizallet, C.; Nicolle, A.; Da Costa, P. Multiscale Modeling of Barium Sulfate Formation from BaO. *Ind. Eng. Chem. Res.* **2013**, *52*, 9086−9098.
(72) Sabbe, M. K.; Reyniers, M.-F.; Reuter, K. First-Principles Kinetic Modeling in Heterogeneous Catalysis: an Industrial Perspective on Best-Practice, Gaps and Needs. *Catal. Sci. Technol.* **2012**, *2*, 2010−2024.
(73) Maestri, M. Escaping the trap of complication and complexity in multiscale microkinetic modelling of heterogeneous catalytic processes. *Chem. Commun.* **2017**, *53*, 10244−10254.
(74) Jasper, A. W.; Pelzer, K. M.; Miller, J. A.; Kamarchik, E.; Harding, L. B.; Klippenstein, S. J. Predictive a Priori Pressure-Dependent Kinetics. *Science* **2014**, *346*, 1212−1215.
(75) Mao, Y.; Wang, H.-F.; Hu, P. Theory and Applications of Surface Micro-Kinetics in the Rational Design of Catalysts using Density Functional Theory Calculations. *Wiley Interdiscip. Rev.: Comput. Mol. Sci.* **2017**, *7*, No. e1321.
(76) Kresse, G.; Hafner, J. Ab Initio Molecular-Dynamics Simulation of the Liquid-Metal-Amorphous-Semiconductor Transition in Germanium. *Phys. Rev. B* **1994**, *49*, 14251−14269.
(77) Kresse, G.; Furthmüller, J. Efficiency of Ab-Initio Total Energy Calculations for Metals and Semiconductors using a Plane-Wave Basis Set. *Comput. Mater. Sci.* **1996**, *6*, 15−50.
(78) Kresse, G.; Joubert, D. From Ultrasoft Pseudopotentials to the Projector Augmented-Wave Method. *Phys. Rev. B* **1999**, *59*, 1758−1775.
(79) Perdew, J. P.; Burke, K.; Ernzerhof, M. Generalized Gradient Approximation Made Simple. *Phys. Rev. Lett.* **1996**, *77*, 3865−3868.
(80) Sanville, E.; Kenny, S. D.; Smith, R.; Henkelman, G. Improved Grid-Based Algorithm for Bader Charge Allocation. *J. Comput. Chem.* **2007**, *28*, 899−908.
(81) Henkelman, G.; Arnaldsson, A.; Jonsson, H. A Fast and Robust Algorithm for Bader Decomposition of Charge Density. *Comput. Mater. Sci.* **2006**, *36*, 354−360.
(82) Digne, M.; Sautet, P.; Raybaud, P.; Euzen, P.; Toulhoat, H. Hydroxyl Groups on Gamma-Alumina Surfaces: a DFT Study. *J. Catal.* **2002**, *211*, 1−5.
(83) Digne, M.; Sautet, P.; Raybaud, P.; Euzen, P.; Toulhoat, H. Use of DFT to Achieve a Rational Understanding of Acid−Basic Properties of Gamma-Alumina Surfaces. *J. Catal.* **2004**, *226*, 54−68.
(84) Jahel, A.; Moizan-Baslé, V.; Chizallet, C.; Raybaud, P.; Olivier-Fourcade, J.; Jumas, J. C.; Avenier, P.; Lacombe, S. Effect of Indium-Doping of Gamma-Alumina on the Stabilization of PtSn Alloy Clusters Prepared by Surface Organostannic Chemistry. *J. Phys. Chem. C* **2012**, *116*, 10073−10083.
(85) Henkelman, G.; Jonsson, H. Improved Tangent Estimate in the Nudged Elastic Band Method for Finding Minimum Energy Paths and Saddle Points. *J. Chem. Phys.* **2000**, *113*, 9978−9985.
(86) Fleurat-Lessard, P.; Dayal, P. Reaction Path Construction and Determination. http://pfleurat.free.fr/ReactionPath.php (accessed April 2, 2016).
(87) Pulay, P. Convergence Acceleration of Iterative Sequences. The Case of SCf Iteration. *Chem. Phys. Lett.* **1980**, *73*, 393−398.
(88) *Chemkin-Pro 15131, Reaction Design*; San Diego, CA, 2013.
(89) Keppeler, M.; Bräuning, G.; Radhakrishnan, S. G.; Liu, X.; Jensen, C.; Roduner, E. Reactivity of Diatomics and of Ethylene on Zeolite-Supported 13-Atom Platinum Nanoclusters. *Catal. Sci. Technol.* **2016**, *6*, 6814−6823.
(90) Hopster, H.; Ibach, H.; Comsa, G. Catalytic Oxidation of Carbon Monoxide on Stepped Platinum(111) Surfaces. *J. Catal.* **1977**, *46*, 37−48.
(91) Bonzel, H. P.; Ku, R. On the Kinetics of Oxygen Adsorption on a Pt(111) Surface. *Surf. Sci.* **1973**, *40*, 85−101.
(92) Lagauche, M.; Larmier, K.; Jolimaitre, E.; Barthelet, K.; Chizallet, C.; Favergeon, L.; Pijolat, M. Thermodynamic Characterization of the Hydroxyl Group on the γ-Alumina Surface by the Energy Distribution Function. *J. Phys. Chem. C* **2017**, *121*, 16770−16782.
(93) Parker, D. H.; Bartram, M. E.; Koel, B. E. Study of High Coverages of Atomic Oxygen on the Pt(111) Surface. *Surf. Sci.* **1989**, *217*, 489−510.
(94) Badan, C.; Farber, R. G.; Heyrich, Y.; Koper, M. T. M.; Killelea, D. R.; Juurlink, L. B. F. Step-Type Selective Oxidation of Platinum Surfaces. *J. Phys. Chem. C* **2016**, *120*, 22927−22935.
(95) Olsson, L.; Westerberg, B.; Persson, H.; Fridell, E.; Skoglundh, M.; Andersson, B. A Kinetic Study of Oxygen Adsorption/Desorption and NO Oxidation over Pt/Al_2O_3 Catalysts. *J. Phys. Chem. B* **1999**, *103*, 10433−10439.
(96) Mihai, O.; Creaser, D.; Olsson, L. Adsorption and Oxidation Investigations over Pt/Al_2O_3 Catalyst: A Microcalorimetric Study. *Catalysts* **2016**, *6*, 73.
(97) Wartnaby, C. E.; Stuck, A.; Yeo, Y. Y.; King, D. A. Microcalorimetric Heats of Adsorption for CO, NO, and Oxygen on Pt{110}. *J. Phys. Chem.* **1996**, *100*, 12483−12488.
(98) Boudart, M.; Aldag, A.; Benson, J. E.; Dougharty, N. A.; Girvin Harkins, C. On the Specific Activity of Platinum Catalysts. *J. Catal.* **1966**, *6*, 92−99.
(99) Dumesic, J. A.; Rudd, D. F.; Aparicio, L. M.; Rekoske, J. E.; Trevino, A. A. *The Microkinetics of Heterogeneous Catalysis*; American Chemical Society: Washington DC, 1993.
(100) Deutschmann, O.; Behrendt, F.; Warnatz, J. Modelling and Simulation of Heterogeneous Oxidation of Methane on a Platinum Foil. *Catal. Today* **1994**, *21*, 461−470.
(101) Gland, J. L.; Korchak, V. N. The Adsorption of Oxygen on a Stepped Platinum Single Crystal Surface. *Surf. Sci.* **1978**, *75*, 733−750.
(102) Schwaha, K.; Bechtold, E. The adsorption of oxygen on the stepped Pt(S)-[9(111) × (111)] face. *Surf. Sci.* **1977**, *65*, 277−286.

DOI: 10.1021/acs.jpcc.8b09204
J. Phys. Chem. C 2018, 122, 26974−26986